ACS APPLIED MATERIALS & INTERFACES

Research Article

www.acsami.org

In Situ One-Step Synthesis of Hierarchical Nitrogen-Doped Porous Carbon for High-Performance Supercapacitors

Ju-Won Jeon,[†,‡] Ronish Sharma,[†] Praveen Meduri,[†] Bruce W. Arey,[†] Herbert T. Schaef,[§] Jodie L. Lutkenhaus,*[,‡] John P. Lemmon,[†] Praveen K. Thallapally,[§] Manjula I. Nandasiri,[†] Benard Peter McGrail,[†] and Satish K. Nune*[,†]

[†]Energy & Environment Directorate and [§]Fundamental Chemical Sciences DirectoratePacific Northwest National Laboratory, 902 Battelle Boulevard, Richland, Washington 99354, United States

[‡]Artie McFerrin Department of Chemical Engineering, Texas A&M University, 3122 TAMU, College Station, Texas 77843-3122, United States

Supporting Information

ABSTRACT: A hierarchically structured nitrogen-doped porous carbon is prepared from a nitrogen-containing isoreticular metal-organic framework (IRMOF-3) using a self-sacrificial templating method. IRMOF-3 itself provides the carbon and nitrogen content as well as the porous structure. For high carbonization temperatures (950 °C), the carbonized MOF required no further purification steps, thus eliminating the need for solvents or acid. Nitrogen content and surface area are easily controlled by the carbonization temperature. The nitrogen content decreases from 7 to 3.3 at % as carbonization temperature increases from 600 to 950 °C. There is a distinct trade-off between nitrogen content, porosity, and defects in the carbon structure. Carbonized IRMOFs are evaluated as supercapacitor electrodes. For a carbonization temperature of 950 °C, the nitrogen-doped porous carbon has an exceptionally high capacitance of 239 F g^{-1}. In comparison, an analogous nitrogen-free carbon bears a low capacitance of 24 F g^{-1}, demonstrating the importance of nitrogen dopants in the charge storage process. The route is scalable in that multi-gram quantities of nitrogen-doped porous carbons are easily produced.

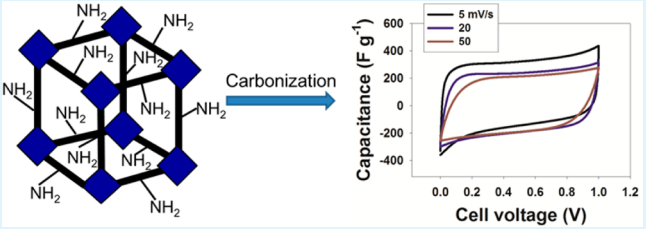

KEYWORDS: *nitrogen-doped porous carbon, supercapacitor, metal-organic framework, energy storage, electrochemistry*

INTRODUCTION

Undoped porous carbons have been commonly used as high-surface-area electrodes in supercapacitors because of their low cost, good processability, and high stability.[1] However, their electrochemical performance has been limited because of the fact that their charge storage mechanism solely depends on the adsorption of electrolyte ions onto the electrode surface.[2] In comparison, nitrogen-doped porous carbons have drawn great attention as electrode materials for energy storage because of their superior electrochemical properties.[3−6] Nitrogen dopants offer an additional mechanism of charge storage known as pseudo-capacitance, in which charge is stored through a rapid surface reaction.[7]

Nitrogen-doped carbons are generally synthesized using complex methods such as chemical vapor deposition (CVD), arc discharge, plasma treatment and thermal annealing with ammonia.[2,8−10] In another approach, carbon precursors were processed with nitrogen-containing precursors (e.g., $CO(NH_2)_2$ and polypyrrole) to produce nitrogen-doped carbons.[3,5,11−13] In these methods, multiple steps were required to mix the carbon and nitrogen precursors and to form the finished product,[8,9,7,11,12]

One promising approach is to utilize precursors that contain both carbon and nitrogen,[14,1516] which reduces the number of steps associated with mixing. Nitrogen-doped carbon has been successfully synthesized using this approach, but there has been limited success in obtaining high surface area product; in one example the surface area was as low as 10 m^2 g^{-1}.[14,16] To increase the surface area, researchers proposed precursor-loaded pore-forming templates.[17−19] Although promising, this approach required additional materials (the pore-forming template) and steps (acid treatment to remove the template).[17−19] Recently, the synthesis of nitrogen-doped porous carbons using ionic liquid-based precursors via direct carbonization was reported.[20−24] The ionic liquid could play the role of carbon source, nitrogen source, and sacrificial pore-forming template.[20−22] However, typical synthesis of the precursor ionic liquids requires multiple steps, and few have been explored as supercapacitor electrodes.[20,25,26]

Crystalline inorganic−organic hybrid materials composed of metal atoms and organic ligands (metal-organic frameworks, or

Received: January 16, 2014
Accepted: April 30, 2014
Published: April 30, 2014

   dx.doi.org/10.1021/am500339x | ACS Appl. Mater. Interfaces 2014, 6, 7214−7222

MOFs) have attracted great attention in various applications including gas separations, catalysis, and energy storage due to the MOF's tunable porosity, functionality, and high surface area.[27] Recently, MOFs were used as templates for the synthesis of porous carbons in which the carbon-containing ligand provides the raw material for carbonization[27−34] Importantly, the MOF itself acts as both the template as well as the carbon source, thus reducing the number of steps required to produce and purify the resulting porous carbon. Conceivably, MOFs bearing nitrogen and carbon-containing ligands could possess similar advantages in that they serve as the carbon source, the nitrogen source, and the template. Therefore, nitrogen-doped porous carbon obtained through the direct carbonization of MOFs is especially promising because it offers a simple approach free of additives and extraneous steps. In an early report, nitrogen-doped porous carbons were possibly fabricated by the carbonization of nitrogen-containing MOFs,[35] but their nitrogen content was not quantified nor discussed. Motivated by the recent interest in porous carbons for supercapacitors, an improvement in the production of high-surface-area nitrogen-doped porous carbons is urgently needed.

Herein, we demonstrate the synthesis of nitrogen-doped porous carbons through the direct carbonization of a nitrogen-containing isoreticular MOF (IRMOF-3). The approach detailed here does not require any additional nitrogen or carbon sources nor does it require an extraneous pore-forming template. Furthermore, the nitrogen content and surface area are simply controlled by altering the carbonization temperature, which was not possible for many prior approaches.[2,10] Both carbonized IRMOF-3 and MOF-5 are evaluated as supercapacitor electrodes. Carbonized MOF-5, which does not contain nitrogen, provides a convenient control to isolate the pseudocapacitance brought by nitrogen dopants in carbonized IRMOF-3, Figure 1. Our route is scalable in that multigram quantities of nitrogen-doped porous carbons are easily produced.

EXPERIMENTAL SECTION

Preparation of Porous Carbons. MOF-5 and IRMOF-3 (isoreticular metal-organic framework-3) were synthesized through simple solvothermal methods reported elsewhere.[37] For the synthesis of MOF-5, zinc nitrate tetrahydrate (3.92 g, 15 mmol) and terephthalic acid (0.83 g, 5 mmol) were added into diethylformamide (150 mL) and sonicated until the solution turned clear. The resulting solution was transferred to an oven held at 105 °C for 24 h. After synthesis, the MOF-5 was washed with diethylformamide several times to remove unreacted precursors.

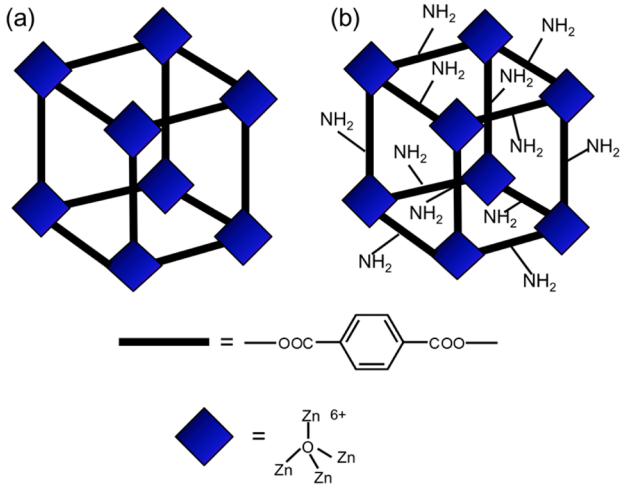

Figure 1. Schematic structure of (a) MOF-5 and (b) IRMOF-3. The structure and drawing concept were adapted from ref 36.

For IRMOF-3, zinc nitrate tetrahydrate (3.92 g, 15 mmol) and 2-aminobenzene-1, 4,-dicarboxylate (0.905 g, 5 mmol) were added to dimethylformamide (150 mL) and sonicated several minutes. The precursor solution was held at 100 °C for 24 h, and the product was then washed with dimethylformamide several times. MOF-5 and IRMOF-3 were immersed in chloroform and stored.

Carbonization. The as-synthesized MOFs were placed in an alumina crucible and then transferred to a tube furnace to undergo carbonization. The furnace was purged with argon gas at room temperature for 1 h. Then the temperature was increased at a rate of 5 °C/min up to 200 °C and maintained at 200 °C for 5 min to remove trace adsorbed contaminants. After 5 min, the temperature was increased at a rate of 1 °C/min to the target temperature (600, 700, 800, or 950 °C). Upon reaching the target temperature, the temperature was maintained an additional 6 h. Then, the furnace was cooled to room temperature at a rate of 2.6 °C/min in the presence of argon. Throughout the procedure, the furnace was continually purged with argon gas. The flow rate of argon gas was 12 ± 2 sccm. The resulting carbon material was ground into a fine powder using a mortar and pestle. The material was then transferred to a scintillation vial for storage.

Characterization. SEM images were obtained using an FEI Helios 600 NanoLab FIB-SEM (focused ion beam−scanning electron microscope). Nitrogen adsorption-desorption isotherms were collected using a Quantachrome autosorb-6 automated gas sorption. Brunauer-Emmett-Teller (BET) surface area was calculated from the nitrogen isotherm curves ranging from 0.1 to 0.3 of relative pressure. Pore size distribution was obtained using a density functional theory (DFT) model. This approach allowed for the measurement of pore diameters ranging from 0.4 to 5.5 nm. Pore diameters below 2 nm were attributed to micropores and those above 2 nm were mesopores. X-ray photoelectron spectroscopy (XPS) was performed using a Kratos Axis Ultra DLD spectrometer, which consisted of a high-performance Al Kα monochromatic x-ray source (1486.7 eV) and a high-resolution spherical mirror analyzer with an energy resolution of 0.1 eV. The X-ray source was operated at 15 kV with an emission current of 10 mA. The charge neutralizer was used to exclude the surface charging effects and the binding energy of C 1s at 284.6 eV was used as the charge reference for binding energy calculations. The composition was determined based on the peak area of existing elements such as carbon, nitrogen, and oxygen using Kratos software. The static contact angle of each electrode was measured using a Rame-Hart goniometer.

Electrochemical Measurements. Electrochemical measurements were carried out in two-electrode symmetric coin cells with 1.0 M sulfuric acid as the aqueous electrolyte. First, the active material was mixed for 30 min with poly(vinylidene fluoride) (PVDF) and conductive carbon black (Super carbon 65, MTI) in *N*-methyl-2-pyrrolidone. The ratio of active materials to conductive carbon black to PVDF was 90:5:5 wt %. After mixing, the slurry was coated onto carbon paper using a brush and dried at 120 °C under vacuum. The prepared electrodes were cut and each electrode was weighed. Typically, the weight of a pair of electrodes was around 1.5 mg. The diameter of an electrode was 1.27 cm^2. The coin cell consisted of a top and bottom metal covering, spring, spacer, separator, two identical electrodes, and the electrolyte. Before measurements, the capacitor cells were soaked in electrolyte overnight so that the active material could be fully infiltrated by the electrolyte. The primary testing being performed was cyclic voltammetry at different scan rates ranging from 5 to 100 mV s^{-1}. Galvanostatic charge/discharge measurements were also carried out at different current rates from 0.5 A g^{-1} to 10 A g^{-1}.

For galvanostatic measurements, the specific capacitances were obtained by using the following equation:[38] $C = 4I\Delta t/(m\Delta V)$. In this equation, C is a specific capacitance (F g^{-1}), I is a current (A), Δt is discharge time (s), m is the mass of two electrodes (g), and ΔV is the

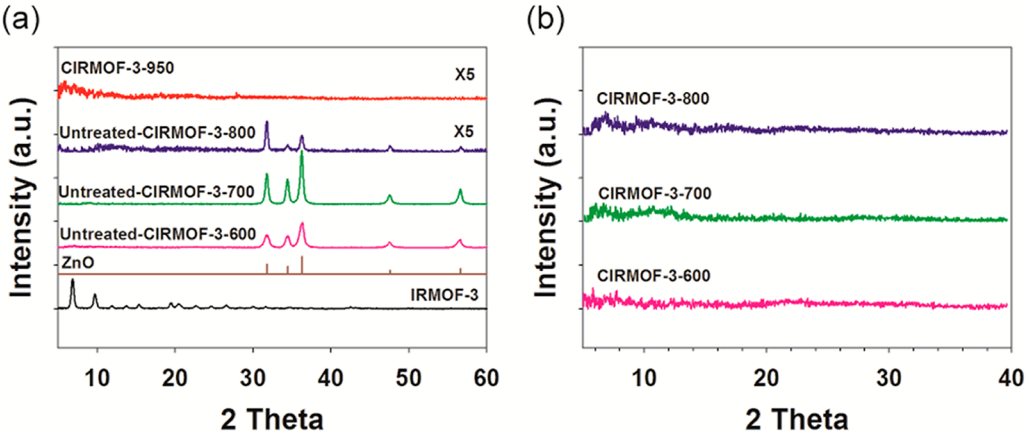

Figure 2. XRD patterns of (a) IRMOF, ZnO, untreated-CIRMOF-3-600, 700, 800, and CIRMOF-950, (b) CIRMOF-3-600, 700, 800 after HCl etching.

Table 1. Physicochemical Properties of Porous Carbons

	S_{BET}[a] (m^2 g^{-1})	total pore volume[b] (cm^3 g^{-1})	micropore volume[b] (cm^3 g^{-1})	mesopore volume[b] (cm^3 g^{-1})	C %	N %	O %	contact angle (deg)
IRMOF-3	1221	0.62	0.6	0.02				
CIRMOF-3-950	553	0.34	0.21	0.13	94.9	3.3	2.8	111
CIRMOF-3-800	402	0.24	0.16	0.08	86.1	3.3	10.6	87
CIRMOF-3-700	454	0.29	0.16	0.13	87.3	6	6.7	78
CIRMOF-3-600	391	0.23	0.15	0.08	85.4	7	7.6	22
untreated-CIRMOF-3-800	124	0.08	0.04	0.04				
untreated-CIRMOF-3-700	158	0.1	0.05	0.05				
untreated-CIRMOF-3-600	319	0.2	0.12	0.08				
CMOF-5-950	572	0.33	0.24	0.09	98.1	-	1.9	138

[a]Brunauer-Emmett-Teller (BET) surface area. [b]Density functional theory (DFT). -Micropore: pore size is less than 2 nm. -Mesopore: pore size is larger than 2 nm and less than 50 nm. In this table, mesopore whose size is less than 5.5 nm is reported.

voltage change during discharge. For cyclic voltammetry, the specific capacitance was taken as $C = (2/m\nu\Delta V) \oint_{V_l}^{V_h} I(V)dV$.[39,40] In this equation, V_h is the high-voltage cut-off, V_l is the low-voltage cut-off, and ν is the scan rate.

RESULTS AND DISCUSSION

MOFs (IRMOF-3,: MOF containing Zn and 2-amino terephthalic acid; MOF-5, MOF containing Zn and terephthalic acid) were prepared using simple solvothermal approaches,[5,41] in which MOF-5 was selected as a nitrogen-free control. The schematic structures of IRMOF-3 and MOF-5 are shown in Figure 1. On the basis of nitrogen adsorption−desorption measurements, the as-synthesized MOFs possessed high surface areas (MOF-5, 1305 m^2 g^{-1}; and IRMOF-3, 1221 m^2 g^{-1}); therefore, carbons derived from these MOFs are expected to have high surface areas and significant differences in nitrogen doping.

To investigate the effect of carbonization temperature on nitrogen content, we carbonized IRMOF-3 at 600, 700, 800, or 950 °C, resulting in carbonized-IRMOF-3, or CIRMOF-3-s. For nomenclature, the carbonization temperature is referred to such that CIRMOF-3-950 indicates a carbonization temperature of 950 °C. MOF-5 was carbonized at 950 °C, resulting in CMOF-5-950. Carbonization of MOFs below 900 °C led to the formation of impurities such as zinc oxide (ZnO). After carbonization, peaks associated with the crystal structure of IRMOF-3 disappeared and peaks associated with ZnO

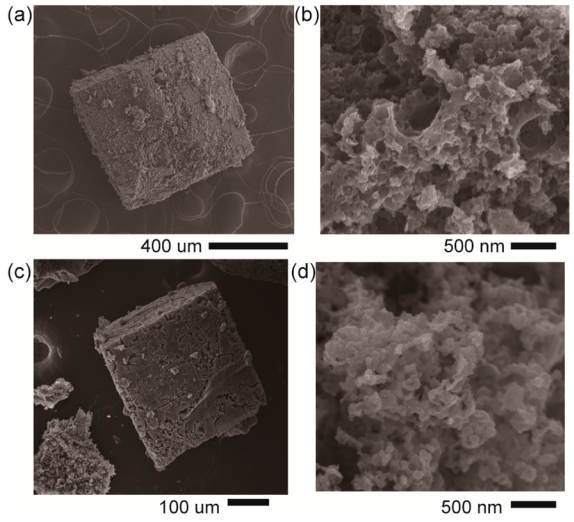

Figure 3. SEM images of (a, b) CIRMOF-3-950 and (c, d) CMOF-5-950.

appeared in XRD patterns (Figure 2a). For the CIRMOF-3 containing ZnO carbonized at 600, 700, and 800 °C, ZnO was removed by HCl etching, Figure 2b. After HCl etching, the surface area and porosity were greatly increased (Table 1). This might be due to the fact that pores were generated while ZnO

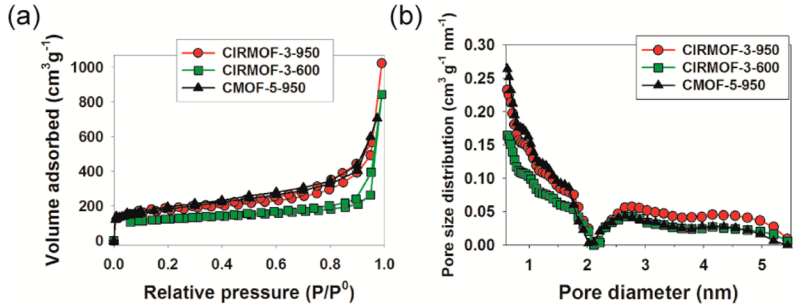

Figure 4. (a) Nitrogen adsorption−desorption isotherms, (b) pore size distribution calculated by density functional theory (DFT).

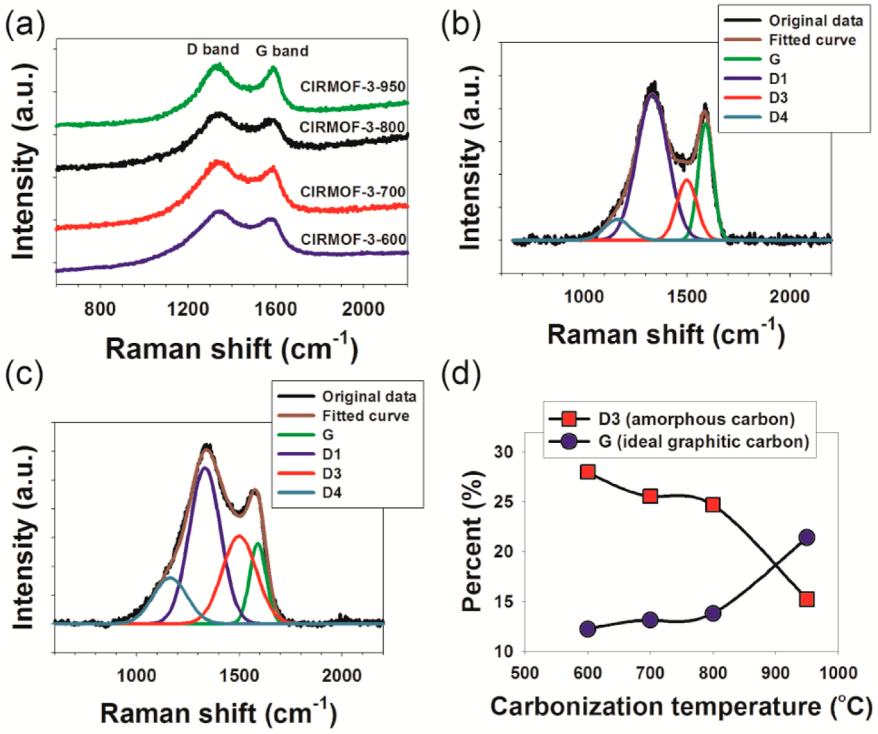

Figure 5. Raman spectra of (a) CIRMOF-3, (b) CIRMOF-3-950, (c) CIRMOF-3-600, and (d) amorphous and ideal graphitic carbon species versus carbonization temperature.

was etched away, possibly acting as an in situ hard template. For carbonization of IRMOF-3 at 950 °C, peaks associated with ZnO disappeared, confirming the sublimation of Zn impurities, resulting in pure carbon. The overall carbon yield of CIRMOF-3-950 was around 17 wt %.

SEM images clearly illustrate the hierarchical porous structure of CIRMOF-3 and CMOF-5, which have a cubic particle shape as well as a porous structure (Figure 3). The rectangular shape is unique to the isoreticular metal-organic framework (IRMOFs), which was maintained during the carbonization process. In Figure 3b, d, it is clear that cubic CMOF particles are composed of interconnected small carbon particles with diameters less than 100 nm. To further characterize its porous nature, the Brunauer−Emmett−Teller (BET) surface area was determined using nitrogen adsorption-desorption measurements. The nitrogen sorption isotherms and pore size distributions of carbons derived from IRMOF-3 and MOF-5 are shown in Figure 4 and Figure S1 in the Supporting Information. CIRMOF-3-950 and CMOF-5-950 both exhibited type I and type II behavior based on the IUPAC classification.[42,43] Both CIRMOF-3 and CMOF-5 showed large uptakes of nitrogen at low relative pressure ($P/P^0 < 0.1$), which was indicative of the presence of abundant micropores. This was followed by a plateau region and a steep increase of adsorbed nitrogen at high relative pressure ($P/P^0 > 0.9$), which probably originated from large meso- and macro pores because of interstitial voids between particles.[42,44]

The pore size distribution was obtained from nitrogen isotherms using density functional theory (DFT).[30,45] The pore size distribution analysis reveals the presence of micropores (< 2 nm) and a good degree of mesoporosity (2−50 nm), Table 1. Both CIRMOF-3-950 and CMOF-950 possess similar total pore volumes (0.34 $cm^3\ g^{-1}$ and 0.33 $cm^3\ g^{-1}$) and surface areas (553 $m^2\ g^{-1}$ and 572 $m^2\ g^{-1}$), respectively. These similarities arise from likenesses between the topology and precursors for IRMOF-3 and MOF-5.[46] As for CIRMOF-3, the high carbonization temperature (950 °C) led to highest micro-, meso-, and total pore volume relative to other carbonization temperatures, as well as the highest surface are. It is possible that Zn sublimation and ligand decomposition during carbonization at 950 °C contributed to the resulting porous structure.[47,48] At low carbonization temperatures, the carbon

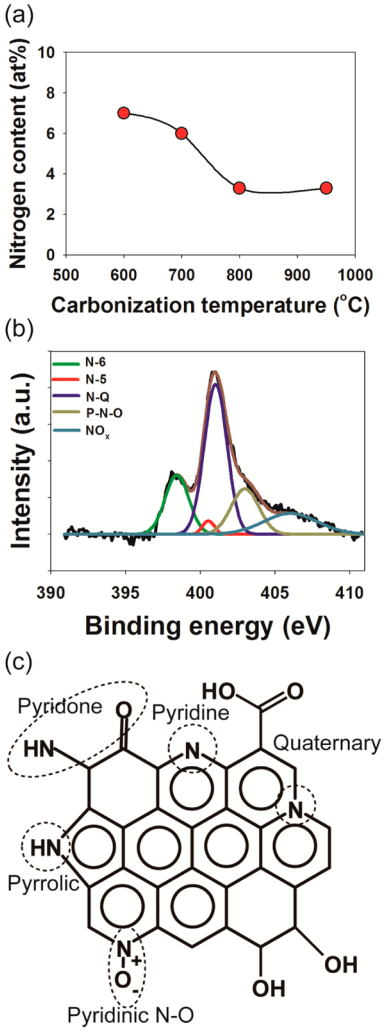

Figure 6. (a) Nitrogen content in CIRMOF-3 with respect to carbonization temperature and (b) the nitrogen region for CIRMOF-3-950 from XPS spectra. (c) Schematic illustration of nitrogen-doped carbon and various nitrogen functionalities identified by XPS.

network may not be fully developed, resulting in a lower surface area and porosity. As the carbonization temperature increases, primary carbon particles likely form interconnected hierarchical structures as shown in images b and d in Figure 3.[30]

Raman spectroscopy was used to investigate the nature of carbon within CIRMOF-3. Two distinctive peaks were observed at 1335 and 1590 cm^{-1}, which correspond to D and G bands, respectively (Figure 5a). The G band indicates ideal graphitic sp^2 carbons, and the D band corresponds to disordered carbons.[49] The average ratios of G to D band intensities (I_G/I_D) for CIRMOF-3-950, CIRMOF-3-800, CIRMOF-3-700, and CIRMOF-3-600 were 0.98, 0.93, 0.94, and 0.89, respectively. CIRMOF-3-950 had the highest I_G/I_D ratio, whereas CIRMOF-3-600 had the lowest I_G/I_D ratio, suggesting that higher carbonization temperatures contributes to the formation of graphitic sp^2 carbons

To more deeply investigate the structural properties of the porous carbons, the Raman spectra were deconvoluted into four different peaks centered at 1590, 1163, 1332, 1499 cm^{-1}, corresponding to G, D1, D3, and D4 bands, respectively, (Figure 5b, c, see Figure S2 in the Supporting Information). D1 and D4 bands indicate disordered graphitic carbon, whereas the D3 band represents amorphous carbon.[50,51] The percentage of amorphous carbon and ideal graphitic sp^2 carbon species versus carbonization temperature are shown in Figure 5d. The percentage of amorphous and ideal graphitic sp^2 carbon was greatly affected by carbonization temperature, in which the percentages of amorphous and ideal graphitic sp^2 carbon species decreased and increased, respectively, with increasing carbonization temperature. We speculate that the abrupt increase in degree of graphitization at 950 °C is related to Zn sublimation during the carbonization process. For CIRMOF-3-950, during the carbonization, Zn sublimation occurs, which could provide carbons with more degree of freedom for graphitization. For CIRMOF-3-600,700, and 800, during carbonization, Zn exists as an oxide form (ZnO), which could lead to hamper overall graphitization process. The results clearly show that higher carbonization temperatures result in a higher percentage of graphitic carbon.[18,52,53]

X-ray photoelectron spectroscopy (XPS) analysis was performed to further quantify the extent of nitrogen doping (Figure 6, Table 1). As carbonization temperature increased from 600 to 950 °C, the nitrogen content decreased from 7 to 3.3 at % for CIRMOF-3, in which nitrogen stems from the decomposition of the 2-aminoterephthalic acid ligand. In comparison, CMOF-5-950 bears no detectable levels of nitrogen, which is not surprising considering it does not contain nitrogen-based ligands. Because the bond energies of C−C and C−N bonds are 370 and 305 kJ,mol^{-1}, respectively, it is highly likely that the C−N bond is more susceptible to cleavage,[54] thus explaining the observed trends with respect to nitrogen content and carbonization temperature. It should also be noted that both MOFs contain oxygen, arising from decomposition of the oxygen-containing ligands.

XPS elemental mapping revealed that nitrogen and oxygen in CIRMOF-3-950 and oxygen in CMOF-5-950 were evenly distributed throughout the porous architecture (see Figure S3 in the Supporting Information). To further characterize the nature of nitrogen in the porous carbons, the N 1s peak of CIRMOF-3-950 was deconvoluted into five different peaks located at 398.4, 400.5, 401, 403, and 406 eV, which were assigned to pyridinic nitrogen (N-6), pyrrolic nitrogen or pyrridone (N-5), quaternary nitrogen (N-Q), pyridine-N-oxide (P−N−O), and chemisorbed NO_x, respectively (Figure 6b, c).[7,55−57] Nitrogen in CIRMOF-3-950 was composed of 19.1% N-6, 2.2% N-5, 46.2% N-Q, 17.2 % P−N−O, and 15.3% NO_x. N-Q was the dominant form of nitrogen in CIRMOF-3-950, whereas the content of N-5 was low. Pyrrolic nitrogen (N-5) has been reported to be less thermally stable than other forms of nitrogen, whereas quaternary nitrogen (N-Q) could be generated from other forms of nitrogen such as pyridinic nitrogen (N-6).[55] Hence, the dominance of N-Q is quite reasonable.

Contact angle measurements were also carried out on CMOF electrodes to assess the wettability of aqueous electrolytes (Table 1). The contact angle of CIRMOF-3-950 was much smaller than that of CMOF-5-950 (111 vs. 138°, respectively), clearly indicating that nitrogen doping increases the electrode's wettability. Besides nitrogen, oxygen-containing functional groups can also contribute to a surface's properties. For CIRMOFs, as carbonization temperature increased, the oxygen content first increased and then decreased. It should be noted that the contact angle was lowest for CIRMOF-3-600, which possessed the highest combined oxygen and nitrogen

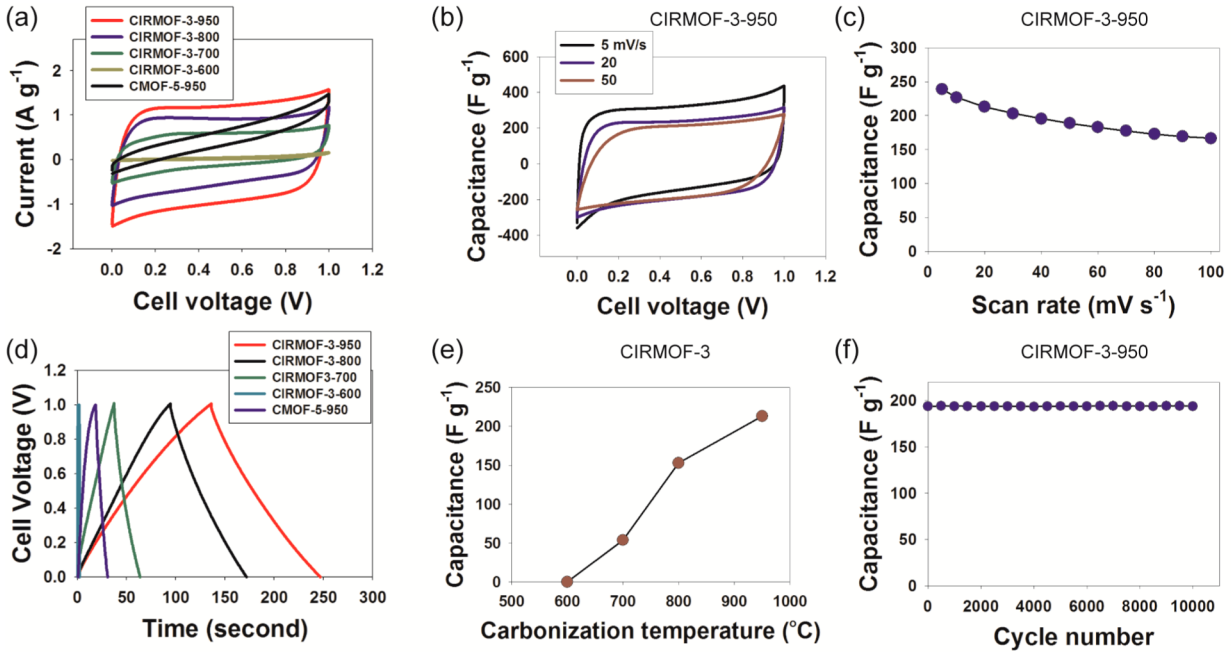

Figure 7. (a) Cyclic voltammograms (CVs) of CMOFs at 20 mV s^{-1}, (b) CVs of CIRMOF-3-950 at different scan rates, (c) specific capacitance of CIRMOF-3-950 vs. scan rate, (d) galvanostatic charge/discharge of CMOFs at 0.5 A g^{-1}, (e) capacitance of CIRMOF-3 vs. carbonization temperature, and (f) cycling of CIRMOF-3-950 at 50 mV s^{-1}.

content, and lowest for CIRMOF-3-950, which possessed the lowest combined oxygen and nitrogen content.

To investigate the electrochemical performance of nitrogen-doped CMOFs as supercapacitors, we prepared electrodes using MOF-derived porous carbons. Symmetric coin cells were assembled using 1 M sulfuric acid as the electrolyte. Electrochemical performance was assessed using cyclic voltammetry and galvanostatic charge/discharge measurements. Figure 7a illustrates typical CVs of CMOFs at 20 mV s^{-1}. The cyclic voltammograms for CIRMOF-3 exhibited a nearly rectangular shape, which is typical behavior for supercapacitors[58,59] for all carbonization temperatures. The CIRMOF-3-950 electrode showed the highest specific capacitance as compared to all other porous carbons investigated even though it had the lowest nitrogen content; presumably this result arises from both CIRMOF-3-950's higher percentage of graphitic carbons as well as its high specific surface area and pore volume.[58] On the other hand, CMOF-5-950 showed distorted CV curves, which might be due to poor electrolyte wettability.[60,61]

The specific capacitance of CIRMOF-3-950 was calculated from the cyclic voltammograms at various scan rates (Figure 7b, c), wherein an excellent specific capacitance of up to 239 F g^{-1} at 5 mV s^{-1} was obtained. Also, the specific capacitance of CIRMOF-3-950 was 189 and 166 F g^{-1} at scan rates 50 and 100 mV s^{-1}, respectively. The good rate capability of CIRMOF-3-950 was attributed to the hierarchical structure, which facilitates electrolyte migration through electrodes.[18]

Galvanostatic charge/discharge measurements were carried out on various CMOFs (Figure 7d, e). Capacitances of 213, 153, 54, 0.3, and 24 F g^{-1} were obtained for CIRMOF-3-950, CIRMOF-3-800, CIRMOF-3-700, CIRMOF-3-600, and CMOF-5-950 at 0.5 A g^{-1}, respectively, see Table S1 in the Supporting Information. Compared to other porous carbons, these values are higher than that of polymerized ionic liquids and lower than that of a nitrogen doped carbon obtained using acetronitrile precursor and zeolite templates, see Table S2 in the Supporting Information.[22,62] It is noteworthy that the specific capacitance of CMOF-5-950 was only 24 F g^{-1}, even though it possessed the highest specific surface area of all CMOFs. The observed electrochemical performance clearly reveals the important role of nitrogen in enhancing electrolyte–electrode interactions and contributing additional pseudocapacitance.[2,63,64]

It should be noted that the capacitance of CIRMOF-3-800 is lower than that of CIRMOF-3-950 even though they possess the same nitrogen content. However, CIRMOF-3-950 possesses a higher percentage of graphitic carbon, which leads to a higher capacitance. Even though CIRMOF-3-800 possesses more oxygen-containing functional groups, which can also potentially contribute to the capacitance,[65,66] far less charge was stored in comparison. This finding suggests that the capacitance depends more on the extent of carbonization than on the oxygen content.

Long-term cycling of CIRMOF-3-950 showed no obvious fade in capacitance even after 10 000 cycles (Figure 7f). Its excellent stability indicates that no major changes in physical or chemical structure occur during the cycling process. Further, the high capacitance and stability of CIRMOF-3-950 suggest its potential in other applications such as oxygen reduction, which we are current exploring.

CONCLUSION

In summary, nitrogen-doped porous carbons were synthesized from MOFs using a self-templating approach without any additional carbon or nitrogen sources. A one-step synthetic route was presented in which no additional purification steps, such as acid washing, were required. In this study, nitrogen content and surface area were easily controlled simply by changing carbonization temperature. Of all the MOFs examined, CIRMOF-3-950 possessed the highest capacitance (239 F g^{-1}) due to an enhanced electrolyte-electrode

interaction, fewer carbon defects, and additional pseudocapacitance from nitrogen dopants. These materials present a straightforward approach to produce porous carbon electrodes, and open new avenues for other applications. Evaluation of nitrogen-doped carbon materials for electrocatalytic activity toward oxygen reduction reaction (ORR) is underway in our laboratory, as is the formation of composite MOF-derived carbon-based electrodes.

■ ASSOCIATED CONTENT

Supporting Information

Nitrogen adsorption−desorption isotherms, pore diameter calculated by density functional theory, Raman spectra, X-ray photoelectron spectroscopy (XPS) element mapping, capacitance at different current density, capacitance of other carbon materials. This material is available free of charge via the Internet at http://pubs.acs.org.

■ AUTHOR INFORMATION

Corresponding Authors

*E-mail: Jodie.lutkenhaus@che.tamu.edu.
*E-mail: Satish.Nune@pnnl.gov.

Notes

The authors declare no competing financial interest.

■ ACKNOWLEDGMENTS

S.K.N. thanks the Pacific Northwest National Laboratory's (PNNL) LDRD program for the support. SEM and XPS characterization were performed at EMSL, a national scientific user facility sponsored by the Department of Energy's Office of Biological and Environmental Research, located at PNNL. J.W.J. thanks PNNL for Internship opportunity. R.S. thanks the Department of Energy (DOE) for a Science Undergraduate Laboratory (SULI) Internship opportunity at PNNL. We thank Paul Martin for his help regarding the use of furnace. We also thank Zemin Nie for nitrogen-sorption measurements. PNNL is a multiprogram national laboratory operated for DOE by Battelle under Contract DE-AC05-76RL01830.

■ REFERENCES

(1) Frackowiak, E.; Beguin, F. Carbon Materials for the Electrochemical Storage of Energy in Capacitors. *Carbon* **2001**, *39*, 937−950.
(2) Jeong, H. M.; Lee, J. W.; Shin, W. H.; Choi, Y. J.; Shin, H. J.; Kang, J. K.; Choi, J. W. Nitrogen-Doped Graphene for High-Performance Ultracapacitors and the Importance of Nitrogen-Doped Sites at Basal Planes. *Nano Lett.* **2011**, *11*, 2472−2477.
(3) Chen, L. F.; Zhang, X. D.; Liang, H. W.; Kong, M. G.; Guan, Q. F.; Chen, P.; Wu, Z. Y.; Yu, S. H. Synthesis of Nitrogen-Doped Porous Carbon Nanofibers as an Efficient Electrode Material for Supercapacitors. *ACS Nano* **2012**, *6*, 7092−7102.
(4) Wen, Z. H.; Wang, X. C.; Mao, S.; Bo, Z.; Kim, H.; Cui, S. M.; Lu, G. H.; Feng, X. L.; Chen, J. H. Crumpled Nitrogen-Doped Graphene Nanosheets with Ultrahigh Pore Volume for High-Performance Supercapacitor. *Adv. Mater.* **2012**, *24*, 5610−5616.
(5) Lee, Y. H.; Chang, K. H.; Hu, C. C. Differentiate the Pseudocapacitance and Double-Layer Capacitance Contributions for Nitrogen-Doped Reduced Graphene Oxide in Acidic and Alkaline Electrolytes. *J. Power Sources* **2013**, *227*, 300−308.
(6) Nasini, U. B.; Gopal Bairi, V.; Kumar Ramasahayam, S.; Bourdo, S. E.; Viswanathan, T.; Shaikh, A. U. Oxygen Reduction Reaction Studies of Phosphorus and Nitrogen Co-Doped Mesoporous Carbon Synthesized via Microwave Technique. *ChemElectroChem.* **2013**, DOI: 10.1002/celc.201300047.
(7) Hulicova-Jurcakova, D.; Kodama, M.; Shiraishi, S.; Hatori, H.; Zhu, Z. H.; Lu, G. Q. Nitrogen-Enriched Nonporous Carbon Electrodes with Extraordinary Supercapacitance. *Adv. Funct. Mater.* **2009**, *19*, 1800−1809.
(8) Wang, X. R.; Li, X. L.; Zhang, L.; Yoon, Y.; Weber, P. K.; Wang, H. L.; Guo, J.; Dai, H. J. N-Doping of Graphene Through Electrothermal Reactions with Ammonia. *Science* **2009**, *324*, 768−771.
(9) Wei, D.; Liu, Y.; Wang, Y.; Zhang, H.; Huang, L.; Yu, G. Synthesis of N-Doped Graphene by Chemical Vapor Deposition and Its Electrical Properties. *Nano Lett.* **2009**, *9*, 1752−1758.
(10) Panchokarla, L. S.; Subrahmanyam, K. S.; Saha, S. K.; Govindaraj, A.; Krishnamurthy, H. R.; Waghmare, U. V.; Rao, C. N. R. Synthesis, Structure, and Properties of Boron- and Nitrogen-Doped Graphene. *Adv. Mater.* **2009**, *21*, 4726−4730.
(11) Chen, X. Y.; Xie, D. H.; Chen, C.; Liu, J. W. High-Performance Supercapacitor Based on Nitrogen-Doped Porous Carbon Derived from Zinc(II)-bis(8-hydroxyquinoline) Coordination Polymer. *J. Colloid Interface Sci.* **2013**, *393*, 241−248.
(12) Hulicova, D.; Yamashita, J.; Soneda, Y.; Hatori, H.; Kodama, M. Supercapacitors Prepared from Melamine-based Carbon. *Chem. Mater.* **2005**, *17*, 1241−1247.
(13) Beguin, F.; Szostak, K.; Lota, G.; Frackowiak, E. A Self-Supporting Electrode for Supercapacitors Prepared by One-Step Pyrolysis of Carbon Nanotube/Polyacrylonitrile Blends. *Adv. Mater.* **2005**, *17*, 2380−2384.
(14) Zhao, L.; Baccile, N.; Gross, S.; Zhang, Y. J.; Wei, W.; Sun, Y. H.; Antonietti, M.; Titirici, M. M. Sustainable Nitrogen-Doped Carbonaceous Materials from Biomass Derivatives. *Carbon* **2010**, *48*, 3778−3787.
(15) Zhao, L.; Fan, L. Z.; Zhou, M. Q.; Guan, H.; Qiao, S. Y.; Antonietti, M.; Titirici, M. M. Nitrogen-Containing Hydrothermal Carbons with Superior Performance in Supercapacitors. *Adv. Mater.* **2010**, *22*, 5202−5206.
(16) Kucinska, A.; Cyganiuk, A.; Lukaszewicz, J. P. A Microporous and High Surface Area Active Carbon Obtained by the Heat-Treatment of Chitosan. *Carbon* **2012**, *50*, 3098−3101.
(17) Olejniczak, A.; Lezanska, M.; Wloch, J.; Kucinska, A.; Lukaszewicz, J. P. Novel Nitrogen-Containing Mesoporous Carbons Prepared from Chitosan. *J. Mater. Chem. A* **2013**, *1*, 8961−8967.
(18) Li, Z.; Xu, Z. W.; Tan, X. H.; Wang, H. L.; Holt, C. M. B.; Stephenson, T.; Olsen, B. C.; Mitlin, D. Mesoporous Nitrogen-Rich Carbons Derived from Protein for Ultra-High Capacity Battery Anodes and Supercapacitors. *Energy Environ. Sci.* **2013**, *6*, 871−878.
(19) Zhu, X.; Hillesheim, P. C.; Mahurin, S. M.; Wang, C. M.; Tian, C. C.; Brown, S.; Luo, H. M.; Veith, G. M.; Han, K. S.; Hagaman, E. W.; Liu, H. L.; Dai, S. Efficient CO2 Capture by Porous, Nitrogen-Doped Carbonaceous Adsorbents Derived from Task-Specific Ionic Liquids. *ChemSusChem* **2012**, *5*, 1912−1917.
(20) Lee, J. S.; Wang, X. Q.; Luo, H. M.; Dai, S. Fluidic Carbon Precursors for Formation of Functional Carbon under Ambient Pressure Based on Ionic Liquids. *Adv. Mater.* **2010**, *22*, 1004−1007.
(21) Lee, J. S.; Wang, X. Q.; Luo, H. M.; Baker, G. A.; Dai, S. Facile Ionothermal Synthesis of Microporous and Mesoporous Carbons from Task Specific Ionic Liquids. *J. Am. Chem. Soc.* **2009**, *131*, 4596−4597.
(22) Fulvio, P. F.; Hillesheim, P. C.; Oyola, Y.; Mahurin, S. M.; Veith, G. M.; Dai, S. A new Family of Fluidic Precursors for the Self-Templated Synthesis of Hierarchical Nanoporous Carbons. *Chem. Commun.* **2013**, *49*, 7289−7291.
(23) Yuan, J.; Marquez, A. G.; Reinacher, J.; Giordano, C.; Janek, J.; Antonietti, M. Nitrogen-Doped Carbon Fibers and Membranes by Carbonization of Electrospun Poly(ionic liquid)s. *Polym. Chem.* **2011**, *2*, 1654−1657.
(24) Zhao, Q.; Fellinger, T. P.; Antonietti, M.; Yuan, J. Y. A. Novel Polymeric Precursor for Micro/Mesoporous Nitrogen-Doped Carbons. *J. Mater. Chem. A* **2013**, *1*, 5113−5120.
(25) Fei, Z. F.; Zhao, D. B.; Pieraccini, D.; Ang, W. H.; Geldbach, T. J.; Scopelliti, R.; Chiappe, C.; Dyson, P. J. Development of Nitrile-Functionalized Ionic Liquids for C-C Coupling Reactions: Implication

of Carbene and Nanoparticle Catalysts. *Organometallics* **2007**, *26*, 1588−1598.
(26) Fei, Z.; Geldbach, T. J.; Zhao, D.; Dyson, P. J. From Dysfunction to Bis-function: On the Design and Applications of Functionalised Ionic Liquids. *Chem.—Eur. J.* **2006**, *12*, 2122−2130.
(27) Li, S.-L.; Xu, Q. Metal-Organic Frameworks as Platforms for Clean Energy. *Energy Environ. Sci.* **2013**, *6*, 1656−1683.
(28) Liu, B.; Shioyama, H.; Jiang, H. L.; Zhang, X. B.; Xu, Q. Metal-Organic Framework (MOF) as a Template for Syntheses of Nanoporous Carbons as Electrode Materials for Supercapacitor. *Carbon* **2010**, *48*, 456−463.
(29) Liu, B.; Shioyama, H.; Akita, T.; Xu, Q. Metal-Organic Framework as a Template for Porous Carbon Synthesis. *J. Am. Chem. Soc.* **2008**, *130*, 5390.
(30) Chaikittisilp, W.; Hu, M.; Wang, H. J.; Huang, H. S.; Fujita, T.; Wu, K. C. W.; Chen, L. C.; Yamauchi, Y.; Ariga, K. Nanoporous Carbons Through Direct Carbonization of a Zeolitic Imidazolate Framework for Supercapacitor Electrodes. *Chem. Commun.* **2012**, *48*, 7259−7261.
(31) Torad, N. L.; Hu, M.; Kamachi, Y.; Takai, K.; Imura, M.; Naito, M.; Yamauchi, Y. Facile Synthesis of Nanoporous Carbons with Controlled Particle Sizes by Direct Carbonization of Monodispersed ZIF-8 Crystals. *Chem. Commun.* **2013**, *49*, 2521−2523.
(32) Xia, W.; Qiu, B.; Xia, D. G.; Zou, R. Q., Facile Preparation of Hierarchically Porous Carbons from Metal-Organic Gels and Their Application in Energy Storage. *Sci. Rep* **2013**, *3*.
(33) Xu, G.; Ding, B.; Shen, L.; Nie, P.; Han, J.; Zhang, X. Sulfur Embedded in Metal Organic Framework-Derived Hierarchically Porous Carbon Nanoplates for High Performance Lithium-Sulfur Battery. *J. Mater. Chem. A* **2013**, *1*, 4490−4496.
(34) Amali, A. J.; Sun, J.-K.; Xu, Q. From Assembled Metal-Organic Framework Nanoparticles to Hierarchically Porous Carbon for Electrochemical Energy Storage. *Chem. Commun.* **2014**, *50*, 1519−1522.
(35) Jiang, H.-L.; Liu, B.; Lan, Y.-Q.; Kuratani, K.; Akita, T.; Shioyama, H.; Zong, F.; Xu, Q. From Metal−Organic Framework to Nanoporous Carbon: Toward a Very High Surface Area and Hydrogen Uptake. *J. Am. Chem. Soc.* **2011**, *133*, 11854−11857.
(36) Ranocchiari, M.; van Bokhoven, J. A. Catalysis by Metal-Organic Frameworks: Fundamentals and Opportunities. *Phys. Chem. Chem. Phys.* **2011**, *13* (14), 6388−6396.
(37) Yang, S. J.; Kim, T.; Im, J. H.; Kim, Y. S.; Lee, K.; Jung, H.; Park, C. R. MOF-Derived Hierarchically Porous Carbon with Exceptional Porosity and Hydrogen Storage Capacity. *Chem. Mater.* **2012**, *24*, 464−470.
(38) Zhao, X.; Zhang, L. L.; Murali, S.; Stoller, M. D.; Zhang, Q. H.; Zhu, Y. W.; Ruoff, R. S. Incorporation of Manganese Dioxide within Ultraporous Activated Graphene for High-Performance Electrochemical Capacitors. *ACS Nano* **2012**, *6*, 5404−5412.
(39) Bao, L. H.; Zang, J. F.; Li, X. D. Flexible Zn2SnO4/MnO2 Core/Shell Nanocable-Carbon Microfiber Hybrid Composites for High-Performance Supercapacitor Electrodes. *Nano Lett.* **2011**, *11*, 1215−1220.
(40) Stoller, M. D.; Ruoff, R. S. Best Practice Methods for Determining an Electrode Material's Performance for Ultracapacitors. *Energy Environ. Sci.* **2010**, *3*, 1294−1301.
(41) Nune, S. K.; Thallapally, P. K.; Dohnalkova, A.; Wang, C. M.; Liu, J.; Exarhos, G. J. Synthesis and Properties of Nano Zeolitic Imidazolate Frameworks. *Chem. Commun.* **2010**, *46*, 4878−4880.
(42) Li, B. Y.; Yang, X. J.; Xia, L. L.; Majeed, M. I.; Tan, B., Hollow Microporous Organic Capsules. *Sci. Rep.* **2013**, *3*.
(43) Sing, K. S. W.; Everett, D. H.; Haul, R. A. W.; Moscou, L.; Pierotti, R. A.; Rouquerol, J.; Siemieniewska, T. Reporting Physisorption Data for Gas Soild Systems with Special Reference to the Determination of Surface-Area and Porosity (Recommendations 1984). *Pure Appl. Chem.* **1985**, *57*, 603−619.
(44) Wang, G.; Dong, Q.; Ling, Z.; Pan, C.; Yu, C.; Qiu, J. S. Hierarchical Activated Carbon Nanofiber Webs with Tuned Structure Fabricated by Electrospinning for Capacitive Deionization. *J. Mater. Chem.* **2012**, *22*, 21819−21823.
(45) Zhang, P.; Sun, F.; Xiang, Z.; Shen, Z.; Yun, J.; Cao, D. ZIF-Derived In Situ Nitrogen-Doped Porous Carbons as Efficient Metal-Free Electrocatalysts for Oxygen Reduction Reaction. *Energy Environ. Sci.* **2014**, *7*, 442−450.
(46) Eddaoudi, M.; Kim, J.; Rosi, N.; Vodak, D.; Wachter, J.; O'Keeffe, M.; Yaghi, O. M. Systematic Design of Pore Size and Functionality in Isoreticular MOFs and Their Application in Methane Storage. *Science* **2002**, *295*, 469−472.
(47) Khezami, L.; Chetouani, A.; Taouk, B.; Capart, R. Production and Characterisation of Activated Carbon from Wood Components in Powder: Cellulose, Lignin, Xylan. *Powder Technol.* **2005**, *157*, 48−56.
(48) Sharma, R. K.; Wooten, J. B.; Baliga, V. L.; Lin, X. H.; Chan, W. G.; Hajaligol, M. R. Characterization of Chars from Pyrolysis of Lignin. *Fuel* **2004**, *83*, 1469−1482.
(49) Dresselhaus, M. S.; Jorio, A.; Hofmann, M.; Dresselhaus, G.; Saito, R. Perspectives on Carbon Nanotubes and Graphene Raman Spectroscopy. *Nano Lett.* **2010**, *10*, 751−758.
(50) Yang, Z.; Guo, J.; Das, S. K.; Yu, Y.; Zhou, Z.; Abruna, H. D.; Archer, L. A. In Situ Synthesis of Lithium Sulfide-Carbon Composites as Cathode Materials for Rechargeable Lithium Batteries. *J. Mater. Chem. A* **2013**, *1*, 1433−1440.
(51) Sadezky, A.; Muckenhuber, H.; Grothe, H.; Niessner, R.; Poschl, U. Raman Micro Spectroscopy of Soot and Related Carbonaceous Materials: Spectral Analysis and Structural Information. *Carbon* **2005**, *43*, 1731−1742.
(52) Kudin, K. N.; Ozbas, B.; Schniepp, H. C.; Prud'homme, R. K.; Aksay, I. A.; Car, R. Raman Spectra of Graphite Oxide and Functionalized Graphene Sheets. *Nano Lett.* **2008**, *8*, 36−41.
(53) Bai, Y. C.; Rakhi, R. B.; Chen, W.; Alshareef, H. N. Effect of pH-Induced Chemical Modification of Hydrothermally Reduced Graphene Oxide on Supercapacitor Performance. *J. Power Sources* **2013**, *233*, 313−319.
(54) Liu, J. W.; Webster, S.; Carroll, D. L. Temperature and Flow Rate of NH3 Effects on Nitrogen Content and Doping Environments of Carbon Nanotubes Grown by Injection CVD Method. *J. Phys. Chem. B* **2005**, *109*, 15769−15774.
(55) Shrestha, S.; Asheghi, S.; Timbro, J.; Mustain, W. E. Temperature Controlled Surface Chemistry of Nitrogen-Doped Mesoporous Carbon and Its Influence on Pt ORR Activity. *Appl. Catal. A* **2013**, *464−465*, 233−242.
(56) Chen, H. C.; Sun, F. G.; Wang, J. T.; Li, W. C.; Qiao, W. M.; Ling, L. C.; Long, D. H. Nitrogen Doping Effects on the Physical and Chemical Properties of Mesoporous Carbons. *J. Phys. Chem. C* **2013**, *117*, 8318−8328.
(57) Shen, J. M.; Liu, A. D.; Tu, Y.; Foo, G. S.; Yeo, C. B.; Chan-Park, M. B.; Jiang, R. R.; Chen, Y. How Carboxylic Groups Improve the Performance of Single-Walled Carbon Nanotube Electrochemical Capacitors? *Energy Environ. Sci.* **2011**, *4*, 4220−4229.
(58) Rakhi, R. B.; Chen, W.; Cha, D.; Alshareef, H. N. Nanostructured Ternary Electrodes for Energy-Storage Applications. *Adv. Energy Mater.* **2012**, *2*, 381−389.
(59) Rakhi, R. B.; Chen, W.; Cha, D. K.; Alshareef, H. N. High Performance Supercapacitors Using Metal Oxide Anchored Graphene Nanosheet Electrodes. *J. Mater. Chem.* **2011**, *21*, 16197−16204.
(60) Shaijumon, M. M.; Ou, F. S.; Ci, L. J.; Ajayan, P. M. Synthesis of Hybrid Nanowire Arrays and Their Application as High Power Supercapacitor Electrodes. *Chem. Commun.* **2008**, *44*, 2373−2375.
(61) Li, X.; Rong, J.; Wei, B. Electrochemical Behavior of Single-Walled Carbon Nanotube Supercapacitors under Compressive Stress. *ACS Nano* **2010**, *4*, 6039−6049.
(62) Ania, C. O.; Khomenko, V.; Raymundo-Piñero, E.; Parra, J. B.; Béguin, F. The Large Electrochemical Capacitance of Microporous Doped Carbon Obtained by Using a Zeolite Template. *Adv. Funct. Mater.* **2007**, *17*, 1828−1836.
(63) Biel, B.; Blase, X.; Triozon, F.; Roche, S. Anomalous Doping Effects on Charge Transport in Graphene Nanoribbons. *Phys. Rev. Lett.* **2009**, *102*, 096803.

(64) Hou, J. B.; Shao, Y. Y.; Ellis, M. W.; Moore, R. B.; Yi, B. L. Graphene-Based Electrochemical Energy Conversion and Storage: Fuel Cells, Supercapacitors and Lithium Ion Batteries. *Phys. Chem. Chem. Phys.* **2011**, *13*, 15384−15402.
(65) Hyder, M. N.; Lee, S. W.; Cebeci, F. Ç.; Schmidt, D. J.; Shao-Horn, Y.; Hammond, P. T. Layer-by-Layer Assembled Polyaniline Nanofiber/Multiwall Carbon Nanotube Thin Film Electrodes for High-Power and High-Energy Storage Applications. *ACS Nano* **2011**, *5*, 8552−8561.
(66) Lee, S. W.; Yabuuchi, N.; Gallant, B. M.; Chen, S.; Kim, B. S.; Hammond, P. T.; Shao-Horn, Y. High-Power Lithium Batteries from Functionalized Carbon-Nanotube Electrodes. *Nat. Nanotechnol.* **2010**, *5*, 531−537.